Nuclear Magnetic Resonance Imaging of Simulated Voids in Cement Slurries

E. J. Fordham, T. P. L. Roberts, T. A. Carpenter, and L. D. Hall
Herchel Smith Laboratory for Medicinal Chemistry, Cambridge University School of Clinical Medicine, Cambridge CB2 2PZ, England

G. C. Maitland and C. Hall
Schlumberger Cambridge Research Ltd., Cambridge CB3 0HG, England

The initial technological development of nuclear magnetic resonance (NMR) imaging was motivated primarily by applications in medicine and biology (for example, Morris, 1986); however, increasing attention is now being given to applications to nonliving systems such as porous media (Osment et al., 1990) and polymer science (Jackson et al., 1991). These applications place higher demands on hardware performance and ingenuity in imaging protocol design, principally because of the broader linewidths and shorter relaxation times found in such heterogeneous systems compared with those of biological tissues. NMR relaxometry in heterogeneous systems has provided insight into pore sizes, surface area, and molecular dynamics in porous media (Banavar and Schwartz, 1989), suspensions (Fripiat et al., 1982), and hydrating cement (Lasic, 1989). Most of the latter are studies of the ^{1}H (proton) resonance of water in a hydrating slurry. Even for relaxometry, measurements can be difficult in commercial cements (McTavish et al., 1985) because of the short relaxation times typically found. Standard *imaging* experiments are almost unviable; the broad linewidth severely limits the spatial resolution which can be achieved, and in spin-echo techniques (Mansfield and Morris, 1982) the short transverse relaxation time T_2 usually causes severe attenuation of the NMR signal by the time spatially encoded data can be acquired. This conclusion is in opposition to a naive view that the high water content of cement slurries makes them a natural candidate for NMR studies. Nevertheless, with a suitable compromise in material choice and some ingenuity in experiment design, high contrast images of simulated voids in a wet cement slurry can be obtained, as we demonstrate in this work.

By "void" we mean both nonporous solid objects and gas- or vapor-filled bubbles or fissures giving negligible liquid-state proton NMR signal. The motivation of this study was to develop a technique by which movement of gas "voids" within a slurry could be examined experimentally. Natural gas migration is an important failure mode of oil-well cementing operations (Parcevaux et al., 1990). The imaging speeds achieved (down to 5 seconds per slice-selective image) indicate that this technique is feasible for such applications. Other viable applications may be in imaging aggregate distribution or crack detection in model concretes and in ceramic casting, or indeed in void detection in any other proton-containing material with comparable values of its NMR parameters.

Materials

Two cements were examined. The imaging study used a cosmetic white Portland cement "Snowcrete" supplied by Blue Circle Industries PLC. Comparison relaxation measurements on a sample of an oilfield Class G cement were also made. The white cement differs from typical ordinary portland cements (OPC's) in having a very low iron content (less than 0.5% Fe_2O_3 w/w) and a correspondingly higher aluminum content. The silicate contents are very similar. The iron in Portland cements is present predominantly in the +3 oxidation state and is incorporated mainly in aluminoferrite minerals of complex composition (Taylor, 1990). The Fe^{3+} ions are paramagnetic and are responsible for the grey/brown color of OPC's.

The presence of paramagnetic components in a slurry has two effects: (i) nuclear magnetic relaxation of water protons in suspensions and porous media, usually dominated by surface relaxation processes (Banavar and Schwartz, 1989), will be increased by exposure to paramagnetic centers at those surfaces; and (ii) the mismatch of magnetic susceptibility between the paramagnetic solid and the slurry water will create internal magnetic field gradients when the slurry is placed in the magnet of an NMR system (Kleinberg and Horsfield, 1990). The latter effect is responsible for the broad resonance lines observed with OPC's; the water protons suffer *inhomogeneous broadening*. Both effects are responsible for shortening the T_2.

By reducing the iron content, the manufacturer can produce a white cement. For NMR purposes, such cements show longer relaxation times and a narrower ^{1}H resonance in the slurry

E. J. Fordham is on leave from Schlumberger Cambridge Research Ltd.

Table 1. Typical Values of NMR Parameters of Two Commercial Cement Slurries (Water/Cement Ratio 0.44 w/w) Measured at Ambient Conditions about 2 Hours after Mixing, Using the ^{1}H Resonance at 84 MHz*

Material	$\Delta\nu$/Hz (FWHM)	T_2^*/μs	T_2/ms	T_1/ms
Snowcrete	600–1000	320–530	6.3–8	130–140
Class G	2900–5000	65–110	1.4	27

*T_2 data acquired at echo spacings of 728 μs and 200 μs, respectively, using the Carr-Purcell-Meiboom-Gill sequence.

than for OPC's. Typical values are shown in Table 1, with values for an oilfield Class G cement shown for comparison. Linewidth and relaxation rates still make even the white cement a "difficult" material for NMR imaging. The relaxation times also develop as the cement hydrates. This is shown in Figure 1 for the white slurry used. The times plotted are derived by fitting to a stretched exponential model $\{\exp[-(\tau/T_{2,1})^{\alpha}]\}$, and the stretching exponent is also plotted. In fact, this was nearly unity over most of the hydration period, in agreement with Blinc et al. (1989). Also shown is the magnetization M_0 derived from the T_2 data. Figure 1 shows that the spin-lattice relaxation time T_1 falls off significantly faster than T_2; and M_0, in fact, changes little over this period. There is suspicion in the literature (McTavish et al., 1985) that part of the water proton content in a hydrating cement may have relaxation times so short that it is "invisible" to normal liquid state NMR techniques. M_0 here does not necessarily represent *total* water content; however, it does represent the maximum signal available in a spin-echo imaging experiment. For imaging, long T_2 values are generally desirable for sufficient signal to noise ratio in the echoes, while long T_1 values are detrimental, as they limit the scan repetition rate which can be achieved. A practical consequence of Figure 1 is that the relative evolution of T_1 and T_2 is favorable for imaging up to about 6 hours after hydration; and this is beyond the so-called "thickening time" of this cement of about 3 hours.

NMR Imaging Protocol

The NMR pulse sequence used is shown schematically in Figure 1. Image slice selection is accomplished by the use of a specially-shaped radio-frequency (RF) excitation pulse in conjunction with the linear field gradient G_y. The RF pulse (which we call a "prefocused" pulse) was designed using simulated annealing (Kirkpatrick et al., 1983) to be sharply band-selective with minimal phase dispersion at the end of the pulse. The shape shown is schematic only; in reality, both amplitude and phase modulation are highly complex and irregular. It has a superior slice-definition profile to the sin t/t profile commonly used for slice selection (Mansfield and Morris, 1982) and requires no gradient lobe after the pulse to refocus phase dispersion present in the excitation after a sin t/t pulse. Details are given by Roberts et al. (1990).

In-plane spatial encoding is achieved in the standard Fourier imaging manner (Morris, 1986): in one direction by frequency encoding by gradient G_z and in the other by phase encoding by gradient G_x. In this experiment, spin echoes are digitized after the application of a 180° refocusing pulse.

The magnitude double Fourier transform of the resulting data set forms a 128^2 pixel image. The design of this sequence offers the following advantages:

- The use of a "hard" refocusing pulse allows for a short echo time T_E (Figure 2), in this case 2.99 ms. To minimize attenuation by transverse relaxation, we require $T_E \leq T_2$. T_2 values in Table 1 show that this T_E should give usable results for Snowcrete, but not for the Class G cement examined.
- The "prefocused" character of the shaped pulse means that no gradient lobe to refocus out of phase spins is required.
- The prefocused pulse has the property of dephasing or "spoiling" transverse coherence existing prior to the application of the pulse. This means that it is unnecessary to wait several times T_1 for repolarization of the specimen after each acquisition. Subject to adequate signal, rapid scan repetitions can be performed with signal weighted as $1 - \exp(-T_R/T_1)$, where T_R is the scan repeat time. The logical extreme of this is the "prefocused FLASH" technique (Roberts et al., 1991), which differs from the present sequence only in the use of gradient-recalled echoes that further increase imaging speed. The latter, however, is impractical here because of the cement slurry's short T_2^* (inverse linewidth). Although nearly as fast, the sequence of Figure 1 cannot be used for *rapid* medical

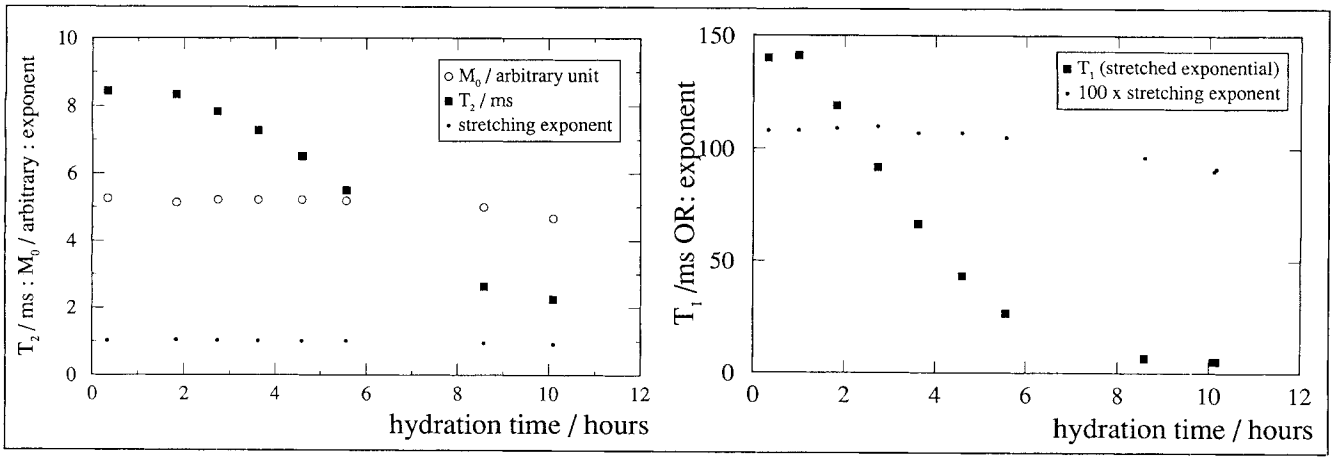

Figure 1. Development of relaxation times T_2 (a) and T_1 (b) with hydration time of the white cement slurry.

Stretching exponents with magnetization M_0 were determined from the T_2 data. The inversion recovery method was used for T_1, the CPMG method for T_2 with an echo spacing of 728 μs.

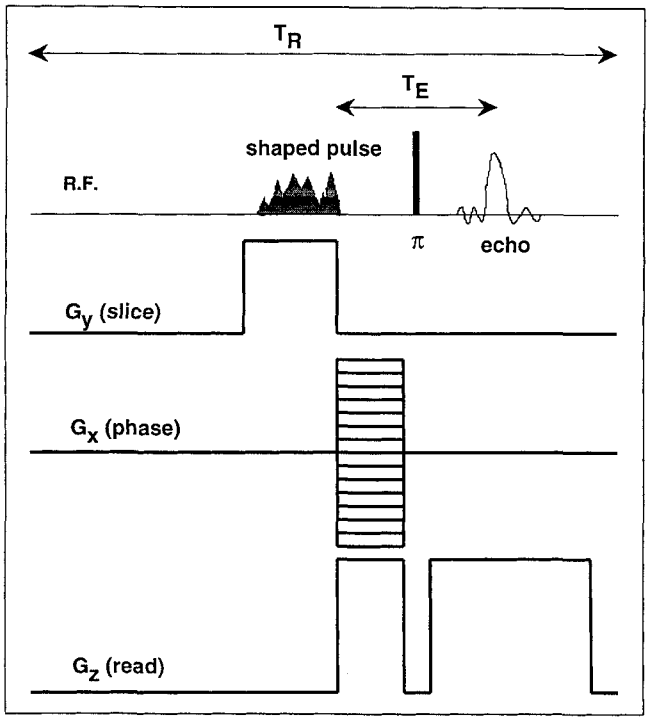

Figure 2. Short echo-time pulse sequence using the "prefocused" slice selective pulse.

imaging because of the high RF power deposition from a rapid stream of 180° pulses. This is not a major consideration with nonliving specimens.

• A further property of the prefocused pulse is that transverse magnetization is small until late in the pulse. Details of this will be the subject of a further publication, but the overall effect is that although the pulse is long compared to T_2^* and of comparable magnitude to T_2, the effects of transverse relaxation are strong only over a short period toward the end of the pulse. This helps to preserve available signal. Some out-of-slice excitation is present with broad-line specimens, but not sufficient to degrade high-contrast void detection.

Results

A simple test phantom was prepared using a white cement slurry of water:cement ratio 0.44 w/w. This was placed in a glass bottle and simulated voids created by scrap rod, tube and sheet polymethyl-methacrylate. The test object was mounted inside a split-ring resonator (Hall et al., 1985) of 65-mm ID ^{1}H NMR data were acquired on an Oxford Research Systems Biospec I console at 84 MHz, using an Oxford Instruments 31-cm bore magnet. Home-built 20-cm gradient sets were employed giving gradient strengths up to 38 $mT \cdot m^{-1}$ with rise times of approximately 300 μs.

Acquisition time is roughly $N_A N_\phi T_R$, where N_ϕ is the number of phase-encoded profiles acquired and N_A is the number of signal averages. The limit to speed is set by the ratio T_R/T_1 at which the T_1 weighting of the sequences leaves unacceptably low S/N. Figure 3 shows four images on a common magnitude scale taken at various T_R down to 19 ms; and at this value, the total acquisition time was only 4.9 seconds for 128^2 pixels

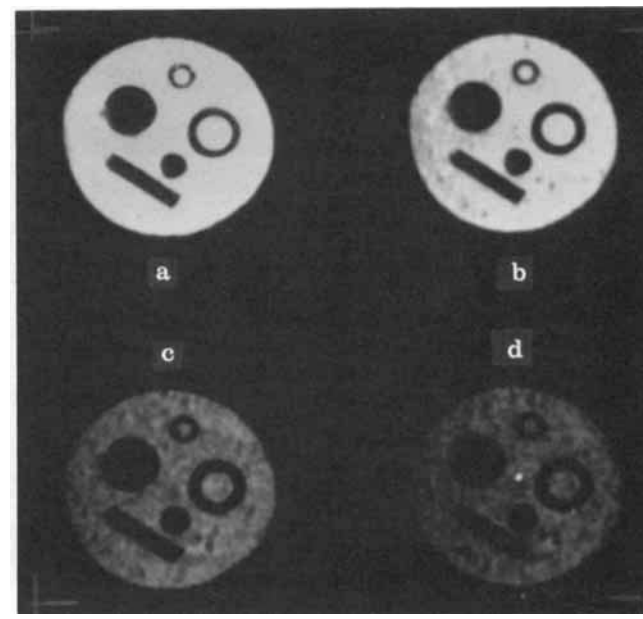

Figure 3. Images of simulated voids in the white cement slurry, about 1 hour after mixing, various scan repetition times T_R.

Slice thickness 5 mm; slice gradient 19 $mT \cdot m^{-1}$ (8,000 $Hz \cdot cm^{-1}$); "prefocused" pulse width 2.5 ms; echo time $T_E = 2.99$ ms; spectral width 100 kHz; read gradient 38 $mT \cdot m^{-1}$ (16,000 $Hz \cdot cm^{-1}$); phase gradient increment 0.37 $mT \cdot m^{-1}$ (160 $Hz \cdot cm^{-1}$), 180° pulse width 53 μs. Gaussian windowing applied to data set; two signal averages; 128^2 pixels interpolated to 512^2. True sizes of objects: Rods 10-mm, 5-mm diameter. Tubes 10-mm, 5-mm O/D, 2-mm, 1-mm wall thickness; slab thickness 3 mm.

Repetition times T_R: (a) 509 ms (b) 89 ms (c) 29 ms (d) 19 ms.

and two signal averages. Physical slice thickness was 5 mm. Two rescaled images are shown with sample horizontal profiles in Figure 4. These show that for void imaging the minimum T_R used still gives acceptable S/N. The 1-mm walls of the small tube are still resolved. In practice, S/N may be good enough not to require averaging to reduce incoherent noise. However, the sequence is prone to develop a "horizontal zipper" artifact (Henkelman and Bronskill, 1987) arising from stimulated echoes caused by errors in the length of the 180° pulse, especially at short T_R. These echoes are successfully eliminated by signal averaging while alternating the phase of the 180° pulse, as was done for the images shown here.

Image Interpretation

All NMR imaging experiments of this type have image intensity biased by relaxation times as well as by local (mobile) proton density ρ. Modeling relaxation by single exponentials (shown to be appropriate by the data of Figure 1), the present experiment yields an image intensity $S(x; T_E, T_R)$ given by:

$$S(x;T_E,T_R) = A\rho(x)\exp[-T_E/T_2(x)]\{1 - \exp[-T_R/T_1(x)]\} + \hat{n}(x) \quad (1)$$

where x is the image co-ordinate and $\hat{n}$ denotes random noise. Variations in T_1 and T_2 can, therefore, cause intensity varia-

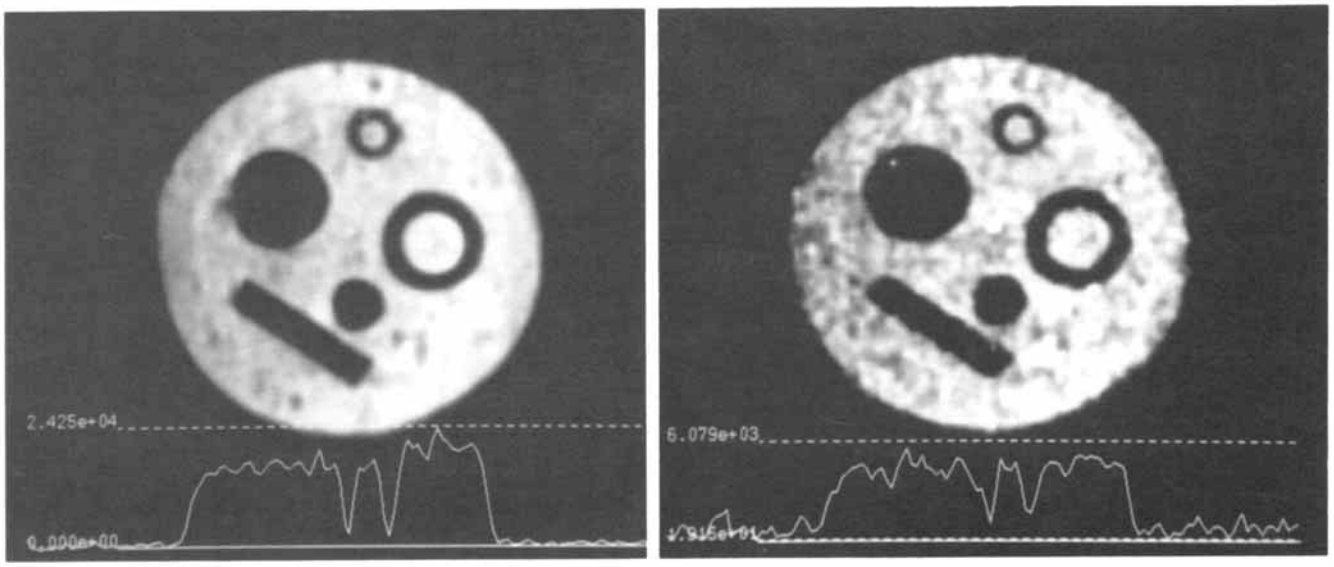

Figure 4. Rescaled images from Figure 3, with sample horizontal profiles through the small tube.

(a) T_R = 509 ms; S/N ≃ 40; total acquisition time 2.2 minutes. (b) T_R = 19 ms; S/N ≃ 8; total acquisition time 4.9 s. Other parameters as for Figure 3.

tions as well as variations in ρ; and where (mean) signal to (RMS) noise ratio $<S>/\sigma_n$ is poor, random variations may also be confused with structural features. In general, interpretation may be a complex matter; however, detection of voids ($\Delta\rho/\rho = 1$) is not particularly sensitive to the relatively mild and smooth local variations in relaxation times expected for an otherwise well-mixed slurry. Consider pixel-to-pixel variations in S arising from a combination of variations in ρ, $T_{2,1}$ and noise n. For random noise uniform and uncorrelated across the image, we find from Eq. 1 that:

$$\frac{\Delta S}{<S>} = \frac{\Delta\rho}{\rho} + \frac{T_E}{T_2}\frac{\Delta T_2}{T_2} - \frac{T_R/T_1}{\exp(T_R/T_1)-1}\frac{\Delta T_1}{T_1} + \frac{\sqrt{2}\sigma_n}{<S>} \qquad (2)$$

The linear dependence of S on ρ gives a fixed sensitivity (unity) of S to fractional variations in ρ. The nonlinear dependence of S on $T_{1,2}$ gives sensitivities to fractional variations in $T_{1,2}$ which depend on the ratios T_E/T_2 and T_R/T_1, as given by the second and third terms of Eq. 2. The final term shows how noise (quantified by signal to RMS noise ratio $<S>/\sigma_n$) limits discrimination of variations in S as genuine features. The sensitivity to T_1 (third term of Eq. 2) is complicated analytically but is monotonic increasing in T_1/T_R, with asymptotes of 0 for $T_1 \ll T_R$, 1 for $T_1 \gg T_R$ and a value of about 0.58 for $T_1 = T_R$. It does not exceed unity for any ratio T_1/T_R.

In our experiments, $T_E/T_2 < 0.5$ for up to about 5 hours hydration time. Sensitivity of S to fractional variations in T_2 is therefore less than half that of the sensitivity to variations in ρ. T_R/T_1 was deliberately varied, between about 5 (Figures 3a and 4a) and 0.2 (Figures 3d and 4b), giving corresponding sensitivities (third term of Eq. 2) of 0.03 and 0.9, respectively. At long T_R, sensitivity of S to variations in T_1 is negligible. At short T_R (rapid imaging), sensitivity to T_1 can be comparable to that to ρ, but this only leads to confusion with genuine voids, if large (approaching 100%) variations in T_1 are present in sharply delineated regions. A more serious consequence of low T_R/T_1 ratios is that signal to noise ratio is globally low; and the final term in Eq. 2 becomes important (relative to the first) and the definition of the edges of genuine voids is degraded (compare Figures 4a and 4b and the line profiles showing noise levels in the "empty" part of the images). When in doubt, the remedy is simple; accumulate more signal averages or increase the T_R and repeat.

Limits on spatial resolution are here set by the linewidth $\Delta\nu$ of the specimen. Fundamental considerations show that the limit of resolution δ is given by:

$$\delta \sim \max\left[\frac{2\pi\Delta\nu}{\gamma G_z}, \Delta z\right] \qquad (3)$$

where γ is the proton magnetogyric ratio and Δz is the pixel width. For broad-line specimens, large "read" gradients G_z are required for the linewidth limit not to dominate. The largest G_z on our system are about 38 $mT \cdot m^{-1}$ (16,000 $Hz \cdot cm^{-1}$); thus, for a linewidth of 1 kHz (Table 1), the linewidth limit is about 0.6 mm. The exact value depends on what precise criterion of "resolution" is adopted. In Figure 3, the smallest reliably resolvable feature is about 1 mm in size, in rough agreement with this estimate. The pixel width Δz in this experiment was 0.49 mm; and the above criterion shows that there is no point in attempting to increase resolution by increasing the number of pixels in the image.

Practical Conclusions for Void Detection

We have defined a "void" as any sharply-defined region which exhibits only noise in its image. This encompasses gas- or vapor-filled bubbles, fissures or cracks, and solid stones

(for example, concrete aggregate) which produce negligible liquid-state proton NMR signal. We show above that where the T_E/T_2 and T_R/T_1 ratios are appropriately chosen, a sharply-defined image region with only noise in its interior may be identified as a void with some confidence, given sufficient $<S>/\sigma_n$ ratio. For voids, contrast ratio in the image is *a priori* high; therefore, interpretation is tolerant of the other relatively mild and smooth heterogeneities in proton density or relaxation times expected in otherwise well-mixed slurries. Prior determination of relaxation times on a bulk specimen, however, is essential to determine appropriate T_E and T_R. In a poorly mixed slurry, very dry regions with low ρ and/or short T_2 could also be seen as "voids," however, they are unlikely to be as sharply delineated. The practical consequence for the strength of structural materials is likely to be similar.

A problem with many cement slurries, even when well-mixed, is sedimentation; "free-water" regions can develop above a sedimenting column with a smooth profile of cement concentration below. Free-water regions are likely to show significantly longer T_1 than the slurry, but also longer T_2 and larger ρ. At short T_R, signal levels will be reduced (relative to the main slurry bulk) because of the low T_R/T_1 ratio, but will be increased because of the higher ρ and longer T_2. Provided T_R is sufficiently long, the free-water regions will show bright, not dark, and can therefore be distinguished from voids, and indeed can be made to show brighter than the slurry bulk, providing "void" and free-water detection in one experiment. The only penalty paid for using a long T_R is image acquisition time.

This work used a cosmetic low-iron white cement, a genuinely commercial structural material, although not one used in oil-well cementing. However, the hydration chemistry is very similar to that of OPC's, and the more rapid hydration kinetics can in any case be adjusted with small quantities of nonparamagnetic retarders [for example, sucrose (*sic*)]. In the oil-well applications, which motivated the study (migration of bubbles or gas-filled fissures), slurry rheology is important and is determined initially by particle size. Rheology can be adjusted by choice of cement powder fineness, adjustment of water/cement ratio, and the addition of polymeric viscosifiers. Although some slurry engineering may thus be required, the use of a low-iron cement as a model system for such studies need not be an artificial exercise, and being low in paramagnetic components allows the use of rapid noninvasive imaging techniques such as that reported here.

Acknowledgment

We thank Dr. Herchel Smith for a generous endowment (L.D.H. & T.A.C.) and research studentship (T.P.L.R.). E.J.F. thanks the Royal Society and the S.E.R.C. (United Kingdom) for an Industrial Fellowship, and Schlumberger for leave of absence.

Literature Cited

Banavar, J. R., and L. M. Schwartz, "Probing Porous Media with Nuclear Magnetic Resonance," *Molecular Dynamics in Restricted Geometries*, p. 273, J. Klafter and J. M. Drake, eds., Wiley, New York (1989).

Blinc, R., G. Lahajnar, S. Žumer, and M. M. Pintar, "NMR Study of the Time Evolution of the Fractal Geometry of Cement Gels," *Phys. Rev. B*, **38**(4), 2873 (1989).

Fripiat, J., J. Cases, M. François, and M. Letellier, "Thermodynamic and Microdynamic Behaviour of Water in Clay Suspensions and Gels," *J. Coll. Int. Sci.*, **89**(2), 378 (1982).

Hall, L. D., T. Marcus, C. Neale, B. Powell, J. Sallos, and S. L. Talagala, "Design of Volume Resonator Probes for NMR Imaging," *J. Magn. Reson.*, **81**, 593 (1985).

Henkelman, R. M., and M. J. Bronskill, "Artifacts in Magnetic Resonance Imaging," *Adv. Mag. Res. in Med.*, **2**(1), 1 (1987).

Jackson, P., N. J. Clayden, N. J. Walton, T. A. Carpenter, L. D. Hall, and P. Jezzard, "Magnetic Resonance Imaging Studies of the Polymerisation of Methylmethacrylate," *Polym. Int.*, **24**, 139 (1991).

Kirkpatrick, S., C. D. Gelatt, Jr., and M. P. Vecchi, "Optimisation by Simulated Annealing," *Sci.*, **220**, 671 (1983).

Kleinberg, R., and M. A. Horsfield, "Transverse Relaxation Processes in Sedimentary Rock," *J. Magn. Reson.*, **88**, 9 (1990).

Lasic, D. D., "NMR Studies of Cement Hydration," *Bull. of Magn. Reson.*, **11**(1/2), 11 (1989).

Mansfield, P., and P. G. Morris, "NMR Imaging in Biomedicine," *Adv. Mag. Res.*, Suppl. 2, Academic Press, New York (1982).

Morris, P. G., *NMR Imaging in Medicine and Biology*, Clarendon Press, Oxford (1986).

McTavish, J. C., L. Miljkovic, M. M. Pintar, R. Blinc, and G. Lahajnar, "Hydration of White Cement by Spin-Grouping NMR," *Cement and Concrete Res.*, **15**, 367 (1985).

Osment, P.A., K. J. Packer, M. J. Taylor, J. J. Attard, T. A. Carpenter, L. D. Hall, N. J. Herrod, and S. J. Doran, "NMR Imaging of Fluids in Porous Solids," *Phil. Trans. (A) Roy. Soc. Lond.*, **333**, 441 (1990).

Parcevaux, P., P. Rae, and P. Drecq, "Prevention of Annular Gas Migration," *Well Cementing*, E. B. Nelson, ed., Elsevier, Amsterdam (1990).

Roberts, T. P. L., T. A. Carpenter, and L. D. Hall, "Design and Application of Prefocused Pulses by Simulated Annealing," *J. Magn. Reson.*, **89**, 595 (1990).

Roberts, T. P. L., T. A. Carpenter, and L. D. Hall, "Elimination of Steady-State Magnetisation in Fast Gradient-Recalled Echo Imaging by the Use of Prefocused Pulses," *J. Magn. Reson.*, **91**, 204 (1991).

Taylor, H. F. W., *Cement Chemistry*, Academic Press, New York (1990).

Manuscript received Aug. 5, 1991, and revision received Oct. 21, 1991.